826

Thin Solid Films, 65 (1980) 331–337
© Elsevier Sequoia S.A., Lausanne—Printed in the Netherlands

ION BEAM ANALYSIS OF DIFFUSION PROCESSES IN A TiC FILM ON WC OBTAINED BY CHEMICAL VAPOUR DEPOSITION*

F. RUDOLF AND C. JACCARD
Institut de Physique, Université de Neuchâtel, Rue A.-L. Breguet 1, CH-2000 Neuchâtel (Switzerland)
L. CHOLLET
Laboratoire suisse de recherches horlogères, Rue A.-L. Breguet 2, CH-2000 Neuchâtel (Switzerland)
(Received April 27, 1979; accepted May 23, 1979)

Concentration profiles have been determined in TiC layers produced by chemical vapour deposition on sintered and single-crystal WC samples by the reaction $^{12}C(d,p)^{13}C$ for carbon and by Rutherford backscattering for titanium and tungsten. Depending on the substrate, the carbon concentration shows a minimum (10–20%) at the TiC/WC interface, with a width between 0.24 and 0.65 μm. The presence of tungsten in TiC and on the surface indicates the occurrence of diffusion during the film formation. During subsequent thermal treatments at 1000 °C, tungsten diffuses in TiC ($5.4 \pm 0.5 \times 10^{-14}$ cm^2 s^{-1}) and carbon in WC (5×10^{-14} cm^2 s^{-1}); both processes occur much faster than expected from extrapolated measurements at higher temperature.

1. INTRODUCTION

Cemented carbide cutting tools are substantially improved by titanium carbide coatings produced by chemical vapour deposition (CVD). Although these tools have been commercially available for several years, some problems still remain concerning the decarburizing of the substrate. This has been investigated by different authors[1–4]. A new technique to improve the quality of the TiC-coated cemented carbide tools further consists in covering them with an aluminium oxide layer using the CVD method. This technique gives good results but some problems concerning the adherence of the aluminium oxide layer have still not been resolved.

In order to investigate these problems, we measured tungsten and carbon depth profiles by Rutherford backscattering (RBS) and with the nuclear reaction $^{12}C(d,p)^{13}C$ respectively. Since the adherence problems of the aluminium oxide layer are possibly related to tungsten contamination at the TiC surface, the tungsten diffusion in the TiC layer was measured. The carbon profiles give information on the decarburized TiC/WC interface. A computer-based iterative method, which uses both energy spectra (RBS and nuclear reaction on carbon) has been developed to evaluate the depth profiles. The strong variations of the stopping power with depth have been correctly accounted for by this method.

* This work has been submitted by F. Rudolf in partial fulfilment of a Ph.D. thesis.

2. EXPERIMENTAL

The following three types of substrate were coated by CVD with titanium carbide: (A) technical cemented tungsten carbide containing 6 wt.% Co and a total of 4–5 wt.% TiC, TaC and NbC, with crystallite sizes of 1.5 μm; (B) cemented tungsten carbide containing less than 0.5 wt.% Co with grain sizes between 1 μm and 25 μm; (C) pure single-crystal WC. All coatings were prepared under the same standard CVD conditions (gases, H_2, $TiCl_4$ and CH_4; 1027 °C; 7 kPa; 10 h). The initial thickness of the coatings was measured either mechanically or with RBS. In order to reduce roughness effects, the specimens of type A and B were carefully mechanically polished before and after TiC deposition. Polishing was necessary in order to obtain coating thicknesses between 1 μm and 2 μm which are accessible to ion beam analysis. The single-crystal samples were only polished before deposition. The roughness of the polished surfaces has been checked with a surface stylus. It is near the detection limit which is about 0.03 μm. In order to study tungsten and carbon diffusion, the cemented WC specimens with low cobalt content (type B) were heated to 1000 °C for 5 or 10 h in a protective hydrogen atmosphere.

The tungsten profiles were measured by RBS using beams of 2.8 MeV He^+ and 1.35 MeV deuterium. The two measurements give complementary information. The measurements with the He^+ beam have good depth resolution and sensitivity for tungsten near the surface. Because of the lower stopping power for deuterium in comparison with He^+, the deuterium measurements have a larger analysing depth. Carbon profiles were measured with the nuclear reaction $^{12}C(d,p)^{13}C$ using a 1.35 MeV deuterium beam. The ion beams with a diameter of 0.5 mm were produced by the 3 MeV Van de Graaff accelerator of the University of Neuchâtel. Backscattered particles were detected at 150° with a 25 mm^2 silicon surface barrier detector (He^+ energy resolution of 12 keV) subtending a solid angle of 3.2 msr. Count rates were kept below 2500 s^{-1} for the RBS measurements and 10^4 s^{-1} for the measurement of carbon profiles. With an electronic pile-up rejection system, these rates allowed us to neglect pile-up effects. The resulting beam currents were between 10 and 40 nA depending on the particle type and on the thickness of the TiC coating.

The evaluation of the energy spectra is complicated by the fact that the stopping power varies markedly with the composition. Therefore the spectra were evaluated by successive approximations. With trial profiles for tungsten, carbon and titanium, we calculated the depth scales for the different cases studied, *i.e.* the energies $E_0'(x)$ before diffusion and $E_1(x)$ at the detector as a function of depth x. The stopping power ε which is a function of energy and composition, and consequently of depth, has been numerically integrated. The semi-empirical stopping power values given by Ziegler and Andersen[5,6] and Bragg's rule have been used. Depth is indicated in area densities (10^{18} atoms cm^{-2} correspond to 0.1 μm).

With this approximate depth scale, we evaluated the carbon profiles with a method similar to that proposed by Schulte[7] and Borders and Harris[8]. The proton energy spectra from the nuclear reaction $^{12}C(d,p)^{13}C$ were corrected for the reaction cross section by comparison with a spectrum measured on a reference sample and for the variation of stopping power with depth. A cemented WC specimen with a low cobalt content and without coating has been used as a reference since stopping power and straggling are similar to those of the TiC/WC samples. The corrected

spectrum N^* is obtained from the relation

$$N_i^* = \frac{N_i\{E_{1i}(x)\}}{N_r\{E_{1r}(\tilde{x})\}} C_i(x) \frac{dE_{1r}(\tilde{x})/dx}{dE_{1i}(x)/dx} \tag{1}$$

where the subscripts i and r refer to the unknown and to the reference sample, C_i is the carbon concentration given as an atomic ratio, N is the number of counts in the proton spectrum at the appropriate energy, dE_1/dx is the stopping power from the depth scale calculation and x and $\tilde{x}$ are the depth in the unknown and in the reference samples, respectively, where the deuteron energies $E_{0i}'(x)$ and $E_{0r}(\tilde{x})$ are equal. Figure 1 shows a typical energy spectrum for the $^{12}C(d,p)^{13}C$ reaction as measured and after correction. The statistical spread of the data points is nearly equal to the width of the dotted line. The corrected energy spectrum has been transformed to a concentration profile using the calculated depth scale and suitable averaging. First trial profiles have been chosen as follows. From the corresponding RBS spectrum, the thickness of the TiC coating and the slope of the tungsten signal at the interface are measured. This allows us to calculate the approximate tungsten, titanium and carbon concentration profiles neglecting decarburization effects at the interface. With these profiles, the proton spectrum is evaluated as described earlier. New tungsten and titanium concentrations are determined, assuming that the decarburized region consists only of tungsten and carbon, and using the fact that the sum of the three concentrations is equal to unity. Consistent results are obtained after a few iterations.

These profiles were used to evaluate the RBS spectra. The contribution from the titanium is calculated and subtracted. The carbon contribution can be neglected since the scattering cross section is much smaller than that for tungsten. The resultant tungsten spectrum is corrected for the variation of scattering cross section and stopping power using the surface conditions as a reference. This yields the relation

$$N^*(E_1) = N(E_1)\left(\frac{E_0'(x)}{E_0}\right)^2 \frac{dE_1(x)/dt}{dE_1(x=0)/dt} \tag{2}$$

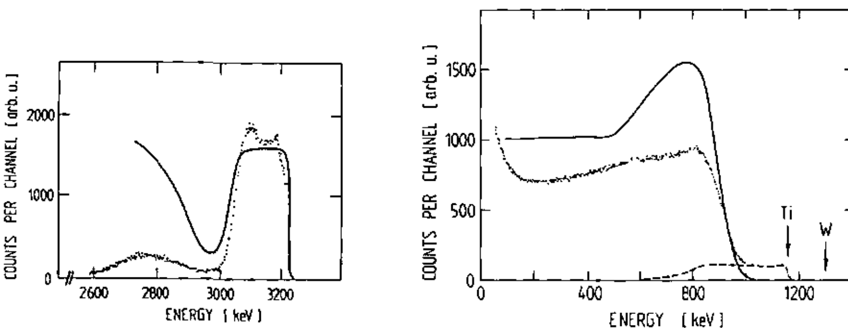

Fig. 1. Typical energy spectrum of a TiC/WC sample from the nuclear reaction $^{12}C(d,p)^{13}C$ (d = 1350 keV): ···, measured spectrum; ——, spectrum corrected for variation of the scattering cross section and stopping power with depth. The thickness of the TiC layer was 1.6 μm.

Fig. 2. RBS spectrum (d = 1350 keV) of a TiC/WC sample and the different steps of the evaluation: ···, measured spectrum; – – –, calculated titanium contribution; ——, tungsten energy spectrum corrected for the variation of scattering cross section and stopping power with depth. The thickness of the TiC layer was 1.6 μm.

where E_0 is the incident energy and x is the scattering depth corresponding to the energy E_1. The various steps of the evaluation are illustrated in Fig. 2. The corrected spectrum is transformed to a depth profile as in the carbon case and is normalized using the titanium spectrum height at the surface. An analogous iteration procedure as in the carbon case has proved to be unnecessary since the result from the second iteration was identical to the first calculation.

Depth resolution is a strongly varying function of depth since it depends on the stopping power (which varies with composition). It was calculated using the depth scale, the energy resolution of the detector and the energy straggling. The energy straggling was estimated as a function of depth with the formula valid for compounds proposed by Chu[9]. The results are indicated in Figs. 4 and 5. No surface roughness effects were included.

3. RESULTS

For the specimens without thermal treatment, the following characteristics are found. The RBS spectra measured on the untreated non-polished samples show a peak corresponding to a small surface layer of tungsten (3×10^{14} cm^{-2}). The tungsten concentration in the TiC layer far from the interface is about 0.03 at.% and it is essentially independent of the depth. At the interface, the tungsten concentration can be described by an exponential: $C_W \propto e^{x/x_0}$ over three decades. This intermediate zone between the TiC layer and the WC substrate can be associated with the mixed carbide layer found by Sharma *et al.*[4] in an electron microscope study. Figure 3 shows that the carbon concentration falls off as the tungsten profile rises. Therefore the intermediate layer is a mixture of TiC and tungsten carbides characteristic of the decarburized region, which occur in the so-called η phase (W_6C, $W_{12}C$, W_6Co_6C, W_3Co_3C). From our measurements it is not possible to distinguish between a mixture at the atomic level or a mixture of different small grains. We note that the zone of mixed carbides is much smaller for the technical sample (A) and the monocrystalline sample (C) than for the low cobalt content sample (B).

The decarburized region can be characterized by the minimal and maximal concentrations of the carbon and tungsten profiles respectively and by the full width

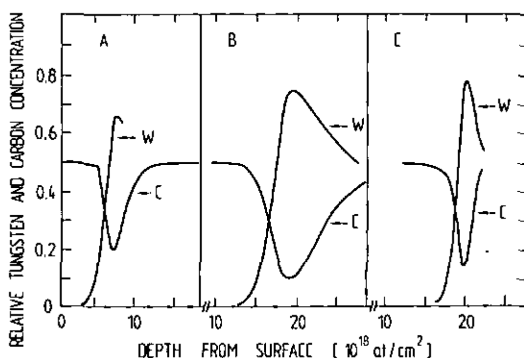

Fig. 3. Tungsten and carbon depth profiles for the different samples without heat treatment: A, technical substrate; B, cemented WC containing less than 0.5 wt.% Co; C, single-crystal WC. The different TiC thicknesses are due to polishing and are not typical for the initial TiC layer.

of the carbon dips measured at half depth. The error on the maximal tungsten concentration is rather large since a change in carbon content does not greatly influence the tungsten RBS spectrum. This contributes to the fact that the sum of the carbon and tungsten concentrations is always less than unity. However, we cannot exclude the possibility of about 5–10 at.% Ti in the decarburized region. The detailed results for the untreated samples are given in Table I.

TABLE I

CHARACTERISTICS OF THE DIFFERENT SPECIMENS AND EXPERIMENTAL RESULTS FOR THE SAMPLES WITHOUT HEAT TREATMENT AT THE INTERFACE

	Type of specimen		
	A	*B*	*C*
Characteristics of the substrate	Co, 6 wt.%	Co < 0.5 wt.%	WC single crystal
Thickness of the deposited layer (μm)	5–6	2.5–3.5	≈2
Tungsten concentration near the surface (at.%)	3×10^{-2}	5×10^{-3}	2×10^{-2}
Tungsten profile e^{x/x_0} at the interface: x_0 (μm)	0.056	0.11	0.062
Minimal carbon concentration (at.%)	20	10	14
Maximal tungsten concentration (at.%)	65	75	78
Full width of the carbon dips at half height (μm)	0.26	0.65	0.24

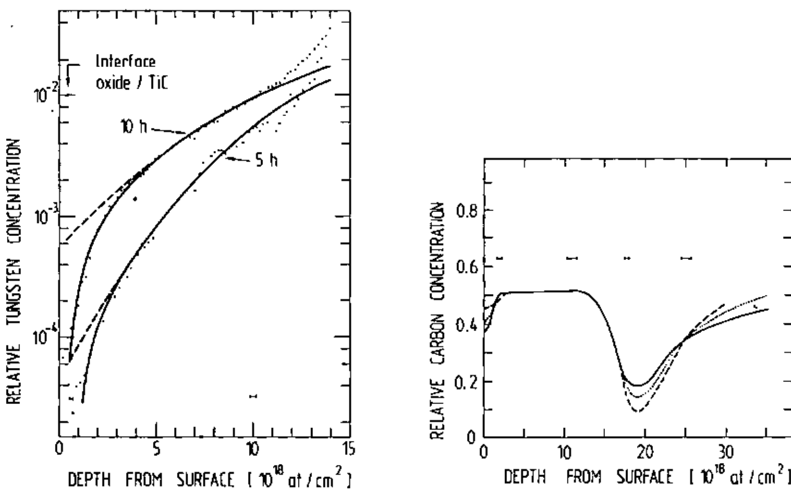

Fig. 4. Diffusion profiles of tungsten in the TiC layer of a TiC/WC sample heat treated at 1000 °C: ——, model with surface sink; – – –, complementary error functions; ···, measured profiles; bars, depth resolution.

Fig. 5. Carbon depth profiles of a TiC/WC sample for different heat treatments on a low cobalt concentration cemented specimen (B): – – –, no treatment; ···, 5 h, 1000 °C; ——, 10 h, 1000 °C; bars, depth resolution.

The concentration profiles of the heat-treated samples are shown in Fig. 4. While the tungsten profiles for concentrations greater than 5 at.% are essentially unchanged, a low concentration diffusion profile appears. We note the sharp drop near the surface which we consider to be due to the formation of an oxide layer at the surface acting as a trap for the tungsten atoms and appearing as a small peak (this peak also contains impurities introduced by the polishing process). The measured profiles are fitted by a model with a constant diffusion coefficient, neglecting the effects of grain boundaries. The tungsten trapped in the oxide layer is lost for diffusion. This is included in the model by requiring the surface concentration to vanish. The fitted curves are shown by full lines in Fig. 4. The corresponding complementary error function which neglects the surface effects is also shown. We find a consistent diffusion coefficient D of $(5.4 \pm 0.5) \times 10^{-14}$ cm^2 s^{-1} and an initial tungsten concentration of 1.5 ± 0.2 at.%. Although the measured profiles are closely fitted by this simple model, we consider that grain boundary diffusion plays an important role and D has to be considered as an apparent diffusion coefficient.

Figure 5 shows the modification of the carbon profile by the heat treatments. An order of magnitude estimate gives an apparent diffusion coefficient $D \approx 5 \times 10^{-14}$ cm^2 s^{-1} for carbon. We note that the redistribution of carbon only takes place in the WC substrate, but as expected no backdiffusion of carbon from the TiC layer is observed.

Samples heated for 2 h at 1200 °C show the same general features as the specimens heated to 1000 °C. Tungsten concentrations up to 10 at.% in the TiC layer are observed. A quantitative evaluation of these measurements was not possible because of important temperature gradients and a strong oxide formation.

4. DISCUSSION AND CONCLUSIONS

The decarburized region is the result of the deposition of the TiC layer. Hintermann *et al.*[1,2] have shown that the carbon necessary for TiC layer formation is provided not only by the methane but also by the substrate. They have also shown that the rate of deposition is proportional to the total carbon supply at the surface. The different thicknesses of TiC layers produced under the same CVD conditions show that the flux of carbon through the TiC layer decreases from the technical to the low cobalt sample and to the single-crystal sample.

In order to explain this result and the measured carbon profiles, the carbon diffusion process in the different samples has to be considered. Two different mechanisms are responsible for carbon transport to the TiC/WC interface:

(1) direct diffusion of carbon in the WC grains;

(2) formation of η carbides (W_6Co_6C, W_3Co_3C) from the binder cobalt and the WC grains and transport of the excess carbon towards the interface.

While diffusion of type (1) can strongly reduce the total carbon content, the depletion is limited by the cobalt content in the second mechanism. We can therefore conclude that the observed carbon dips are mainly due to diffusion of type (1).

In specimens with very little or no cobalt (types B and C) direct diffusion (1) is dominant. The fact that the total carbon flux towards the surface is smaller than in the technical sample shows that in this case the carbon flux is controlled by the substrate. Owing to grain boundary effects carbon diffusion in the cemented sample

is expected to be much faster than in the single-crystal sample. This explains why the carbon dips for the cemented sample are deeper and much larger than for the single crystal. For the technical specimen, the second diffusion mechanism is dominant. Even with a small carbon gradient the diffusion flux towards the interface is strong enough for the carbon flux towards the surface to be limited by diffusion in the TiC layer. Hence the carbon dips are shallower and narrower than for specimen B. Vansant and Phelps[10] have measured the interdiffusion of titanium and carbon. Extrapolation of their results to 1000 °C gives a diffusion coefficient for carbon of 2×10^{-12} cm^2 s^{-1}. This value has to be compared with our apparent diffusion coefficient of 5×10^{-14} cm^2 s^{-1} for carbon in the cemented WC (type B). This confirms our result that in type B samples the diffusion flux of carbon towards the surface is limited by diffusion in the substrate. We note that our apparent diffusion coefficients for tungsten in TiC and carbon in WC are several orders of magnitude larger than those expected from the extrapolation of data measured on single-crystal or quasi-single-crystal samples at higher temperatures[11-13]. This suggests that different mechanisms are active at different temperatures.

During the deposition of titanium carbide layers by CVD two diffusion processes take place.

(1) Carbon diffuses towards the surface, producing a decarburized region which depends markedly on the substrate.

(2) Tungsten diffuses into the TiC layer up to a concentration of the order of 0.03 at.%.

A thermal treatment of several hours at 1000 °C redistributes the carbon in the substrate and induces considerable diffusion of tungsten towards the surface. This tungsten at the surface could influence the subsequent formation of the aluminium oxide layers and this could explain the adherence problems encountered.

ACKNOWLEDGMENTS

This work has been supported by the Swiss National Science Foundation.

REFERENCES

1 H. E. Hintermann, H. Gass and J. N. Lindström, in F. H. Glaski (ed.), *Proc. 3rd Int. Conf. on Chemical Vapour Deposition*, American Nuclear Society, Hinsdale, Ill., 1972, p. 352.
2 H. E. Hintermann and H. Gass, in G. F. Wakefield and J. M. Blocher, Jr., (eds.), *Proc. 4th Int. Conf. on Chemical Vapour Deposition*, The Electrochemical Society, New York, 1973, p. 107.
3 W. D. Sproul and M. H. Richman, *J. Vac. Sci. Technol., 12* (1975) 842.
4 N. K. Sharma, W. S. Williams and R. J. Gottschall, *Thin Solid Films, 45* (1977) 265.
5 H. H. Andersen and J. F. Ziegler, *Hydrogen Stopping Powers and Ranges in All Elements*, Pergamon, New York, 1977.
6 J. F. Ziegler, *Helium Stopping Powers and Ranges in All Elements*, Pergamon, New York, 1977.
7 R. L. Schulte, *Nucl. Instrum. Methods, 137* (1976) 251.
8 J. A. Borders and J. M. Harris, *Nucl. Instrum. Methods, 149* (1978) 279.
9 W. K. Chu, in J. W. Mayer and E. Rimini (eds.), *Ion Beam Handbook for Material Analysis*, Academic Press, New York, 1977, p. 1.
10 C. A. Vansant and W. C. Phelps, Jr., *Trans. Am. Soc. Met., 59* (1966) 105.
11 S. Sarian, *J. Appl. Phys., 39* (1968) 3305.
12 S. Sarian, *J. Appl. Phys., 40* (1969) 3515.
13 C. P. Buhsmer, *Ph.D. Thesis*, Alfred University, Alfred, N.Y., 1968.

10 R. E. Segel, S. S. Hanna and R. G. Allas, *Phys. Rev., Sect. B, 139* (1965) 818.
11 Y. Wada, H. Usui and M. Ashikawa, *Jpn. J. Appl. Phys., 14* (1975) 1351.
12 R. B. Fair, in H. R. Hulf and E. Sirtl (eds.), *Proc. 3rd Int. Symp. on Semiconductor Silicon*, The Electrochemical Society, New York, 1977, p. 968.
13 B. L. Crowder, J. F. Ziegler, F. F. Morehead and G. W. Cole, in B. L. Crowder (ed.), *Ion Implantation in Semiconductors and Other Materials*, Plenum Press, New York, 1973, p. 267.
14 F. J. Morin and J. P. Maita, *Phys. Rev., 96* (1954) 28.
15 R. P. Ricco, J. I. Goldstein and J. G. McCallum, *J. Electrochem. Soc., 124* (1977) 276.
16 S. U. Campisano, G. Foti, E. Rimini and S. T. Picraux, *Nucl. Instrum. Methods, 149* (1978) 371.
17 S. T. Picraux, *J. Appl. Phys., 44* (1973) 587.
18 S. T. Picraux and G. J. Thomas, *J. Appl. Phys., 44* (1973) 594.
19 R. S. Baryshev, V. A. Panteleev and E. I. Akinkina, *Sov. Phys.—Solid State, 16* (1975) 2104.
20 R. S. Baryshev, *Sov. Phys.—Solid State, 19* (1977) 512.

4. DISCUSSION AND CONCLUSION

Numerous transmission electron microscopy and channelling studies have shown that the defect number is much larger in SOS than in bulk silicon[16-18].

The main crystal imperfections are stacking faults, microtwins and dislocations. Channelling analysis of SOS layers demonstrates an increase in stacking faults with increasing depth in the layer. In this work the defect profile was checked by a channelling measurement. The analysis of a silicon layer 0.55 μm thick revealed the same order of magnitude for the stacking fault density as that reported for layers 0.9 μm thick[14], but a somewhat larger gradient of defects.

Baryshev *et al.*[19,20] have shown that vacancy concentration and diffusion are enhanced near dislocations. They have also found that the activation energy for diffusion is lowered by interaction with dislocations. Therefore the boron diffusion enhancement in SOS layers has to be correlated to the defect concentration. Computer simulation with a depth-dependent enhancement factor has not allowed the enhancement to be related to the stacking fault profile in a simple manner.

In conclusion, taking into account its concentration dependence, the boron diffusion in SOS was found to be larger by a factor of 1.1–2.4 than in bulk silicon for temperatures ranging from 900 to 1050 °C. The epitaxial quality is directly responsible for this effect, since diffusion enhancement and defect concentration are both increasing towards the silicon–sapphire interface.

ACKNOWLEDGMENTS

The authors would like to thank Dr. J. P. Thomas and M. Fallavier (Institut de Physique Nucléaire of Lyon, France) for providing the channelling measurement of SOS wafers. Helpful discussions with Dr. H. Luginbühl of the Centre Electronique Horloger S.A. are gratefully acknowledged. The technical assistance of the Centre Electronique Horloger S.A., especially of D. Wüthrich and R. Bachman and of the accelerator group led by J. L. Duport, is greatly appreciated.

This work was partially supported by the Swiss National Science Foundation and the Swiss Foundation of Applied Research. This work was done by F. Rudolf partly to fulfil the requirements of a Ph.D. Thesis.

REFERENCES

1 T. D. Dzhafarov, *Phys. Status Solidi A, 42* (1977) 11.
2 C. D. Maldonado, G. Mandel and G. Kinoshita, *J. Appl. Phys., 47* (1976) 2269.
3 Y. Akasaka, K. Horie, K. Yoneda, T. Sakurai, H. Nishi, S. Kawabe and A. Tohi, *J. Appl. Phys., 44* (1973) 220.
4 R. B. Fair, *J. Electrochem. Soc., 122* (1975) 800.
5 B. Smith, *Ion Implantation Range Data for Silicon and Germanium Device Technologies*, United Kingdom Atomic Energy Authority, Harwell, 1977.
6 R. Schimko, C. E. Richter, K. Rogge, G. Schwarz and M. Trapp, *Phys. Status Solidi A, 28* (1975) 87.
7 A. Armigliato, D. Nobili, P. Ostoja, M. Servidori and S. Solmi, in H. R. Hulf and E. Sirtl (eds.), *Proc. 3rd Int. Symp. on Semiconductor Silicon*, The Electrochemical Society, New York, 1977, p. 638.
8 R. R. Hart and O. J. Marsh, *Appl. Phys. Lett., 15* (1969) 206.
9 G. Dearnaley, J. H. Freeman, R. S. Nelson and J. Stephen, *Ion Implantation*, North-Holland, Amsterdam, 1973, p. 608.

Boundary conditions were given by the fact that no out-diffusion either at the surface[15] or at the silicon–sapphire interface[2] is expected. This implies simply that $dC_B/dx = 0$ at the boundaries.

The results of this calculation for bulk silicon are shown by the broken curves in Fig. 3 and Fig. 4. The experimental results in Fig. 4 for the bulk silicon sample used as reference show good agreement with the calculation. This is not the case for SOS samples, demonstrating that boron diffusion is significantly enhanced. The faster diffusion can be accounted for by introducing an enhancement factor F:

$$D_{SOS}(C_B) = F D_{Si\ bulk}(C_B) \tag{4}$$

Curves calculated with $D_{SOS}(C_B)$ and F as fitting parameter are shown in Fig. 3 and Fig. 4 as full curves. F is found to be between 1.1 and 2.4 for temperatures ranging from 900 to 1050 °C, increasing with increasing diffusion length but practically independent of the implanted dose. This implies that the diffusion enhancement is larger near the silicon–sapphire interface than near the surface since the nominal silicon thickness was the same for all the samples.

Figure 5 shows the mean diffusion coefficients for SOS layers at low boron concentrations, assuming

$$D_{i\ SOS} = F D_{i\ Si\ bulk} \tag{5}$$

for diffusion lengths between 0.18 and 0.34 μm. The activation energy for these mean values is about 2.9 eV which is slightly less than the 3.6 eV value of bulk silicon.

Boron profiles were also calculated with a diffusion model, allowing for an additional diffusion process that is concentration independent. This model is described by

$$D_{SOS}(C_B) = D_{Si\ bulk}(C_B) + D' \tag{6}$$

It was impossible to fit the results which had the same diffusion length but different implanted doses with a single value of D', as expected in such a model.

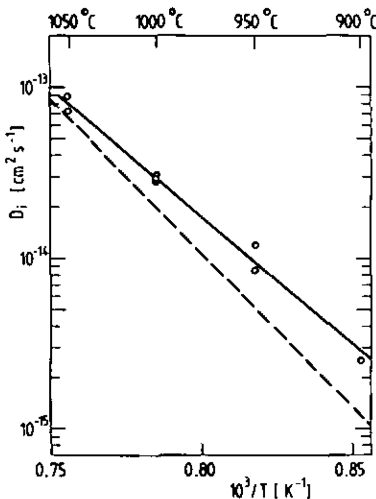

Fig. 5. The mean low concentration boron diffusion coefficient in SOS for diffusion lengths between 0.18 and 0.34 μm: ——, $D_{i\ SOS}$; – – –, $D_{i\ Si\ bulk}$ (ref 4).

The diffusion profiles expected in bulk silicon were calculated with the concentration-dependent diffusion coefficient given by Fair[4]:

$$\frac{D}{D_i} = \frac{p}{n_i} \tag{2}$$

where p is the hole concentration, n_i the intrinsic electron concentration at the diffusion temperature and D_i the boron diffusion coefficient at low concentration. For intrinsic silicon p increases with increasing boron doping; this implies that $p \geqslant n_i$ or $D \geqslant D_i$.

The ratio is temperature independent. This model assumes that boron diffuses by interaction with positively charged vacancies. Diffusion by neutral vacancies cannot be completely neglected, but the theoretical analysis given in ref. 12 and the measurements of ref. 13 show that eqn. (2) is a rather good approximation for the diffusion concentration dependence. For our case, p/n_i is evaluated using $pn = n_i^2$ and the charge neutrality equation. This gives

$$\frac{D(C_B)}{D_i} \approx \frac{C_B}{2n_i} + \left\{ \left(\frac{C_B}{2n_i} \right)^2 + 1 \right\}^{1/2} \tag{3}$$

where C_B is the boron concentration. n_i values were taken from Morin and Maita[14]. The diffusion equation is solved using the finite-difference method. The boron profile is then integrated to make a comparison with the experimental data.

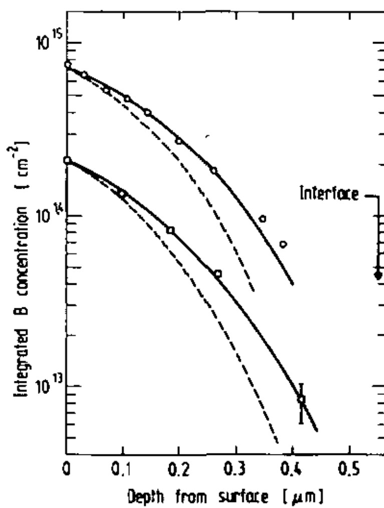

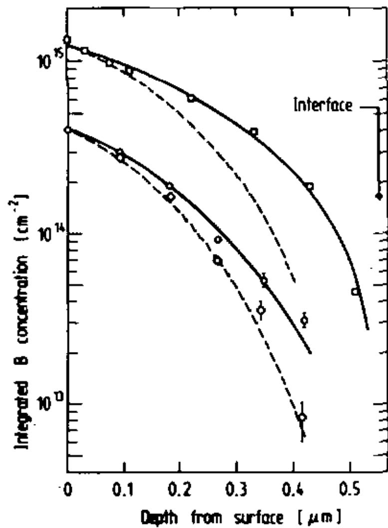

Fig. 3. Experimental and calculated integrated boron profiles: ——, calculated profiles with an enhancement factor $F = 1.7$ (upper curve) and $F = 1.6$ (lower curve) (corresponding diffusion lengths are 0.21 and 0.20 μm respectively); – – –, expected profiles for bulk silicon; ○ and □, SOS, 1000 °C, 1 h.

Fig. 4. Experimental and calculated integrated boron profiles: ——, calculated profiles with an enhancement factor $F = 2.4$ (upper curve) and $F = 1.6$ (lower curve) (corresponding diffusion lengths are 0.33 and 0.23 μm respectively); – – –, expected profiles for bulk silicon; □, SOS, 950 °C, 3.3 h; ○, SOS, 950 °C, 5.2 h; ◇, bulk silicon, 950 °C, 5.2 h (this measurement is given for comparison).

proton absorber foils for α particles from ^{18}O is larger than for those from ^{11}B. This gives an energy separation of about 0.9 MeV for the ^{18}O and ^{11}B signals. By choosing a single-channel analyser window as shown in the figure, the ^{18}O tail is completely eliminated.

Layer removal was performed by ion milling the samples with a 1 keV Ar^+ beam and an etching rate of about 200 Å min^{-1}. Depth steps ranging from 200 to 1000 Å were measured with a surface stylus. Masking during the etching was achieved with Apiezon W. Successive etch steps were made only around the centre of the proton-bombarded area.

Since both the proton and the boron beam power were kept at low values the diffusion due to the heating of the target during bombardments is negligible compared with the diffusion performed at high temperatures[11].

3. RESULTS

Figure 2 shows a typical integrated boron profile as measured. Graphical differentiation averaging the forward and backward differences gives the boron profile itself. The integrated profiles could be well fitted with a complementary error function, except for the highest concentration where the impurity density drops faster at large depths. This demonstrates that the concentration profiles were of a gaussian type. Since the statistical fluctuations are amplified by differentiation the data are analysed in terms of integrated concentration profiles.

An apparent diffusion coefficient can be defined from the broadening of the profile:

$$D_{ap} = \frac{\sigma^2 - \sigma_i^2}{2t} \tag{1}$$

where σ_i^2 and σ^2 are the variances of the gaussian distribution before and after the heat treatment and t is the diffusion time. D_{ap} depends on the implanted dose and temperature as expected and also on the diffusion length $(\sigma^2 - \sigma_i^2)^{1/2}$.

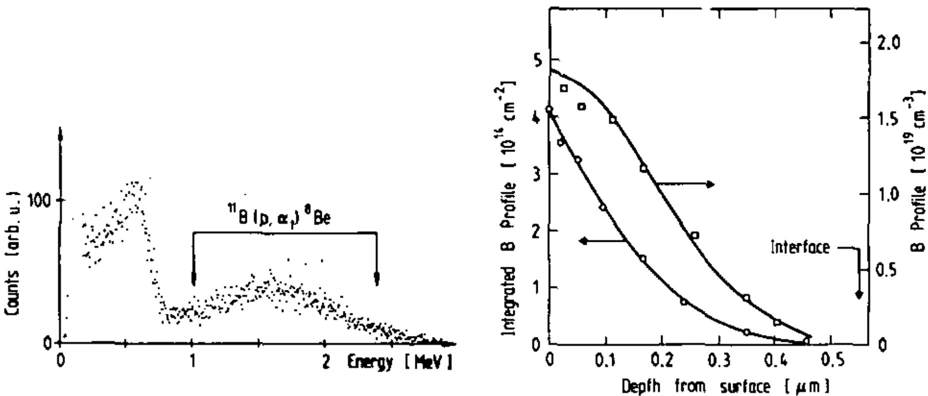

Fig. 1. The energy spectrum obtained by 650 keV proton bombardment of boron-implanted SOS. The arrows indicate the energy window selecting the 3.7 meV α particles slowed down in proton absorber foils. The shoulder at 0.7 MeV is due to 3.3 MeV α particles from the $^{18}O(p,\alpha_0)^{15}N$ reaction in sapphire.

Fig. 2. The boron diffusion profile (1000 °C, 1 h) in SOS (□) found by the differentiation of the measured integrated profile (○).

leads to a half-gaussian distribution in the silicon layer with σ(Si) = 0.052 μm, the maximum being at the silicon surface. The silicon value for straggling can be used, since range and straggling are about the same at 40 keV in SiO_2 and silicon. The profile was checked by measuring an as-implanted sample. Implantation doses in the silicon layer were in the range 2.2×10^{14}–1.4×10^{15} cm^{-2}, which gave peak concentrations in the range 3.3×10^{19}–2.2×20^{20} cm^{-3}. Only for the highest implantation dose were initial peak concentrations slightly higher than the boron solubility[7]. For random implants at room temperature with 40 keV boron ions the dose of 10^{15} cm^{-2} is one order of magnitude smaller than the dose required to produce an amorphous layer[8].

Defect annealing and full boron activation can be obtained at 900 °C[9], *i.e.* below the temperatures for which diffusion was conducted. After oxide etching the diffusion was conducted at temperatures ranging from 900 to 1050 °C in a nitrogen ambient. Diffusion lengths amounted typically to five times the width of the implanted layer and to one-third of the silicon layer thickness.

Boron profiles were obtained by measuring the total amount of ^{11}B in the sample after successive layer removal. ^{11}B is the main isotope (80%) of natural boron, so mass separation during the implantation was not necessary. The analysis was performed with a proton beam from the 0.95–3 MeV University of Neuchâtel Van de Graaff accelerator using the $^{11}B(p,\alpha_1)^8Be$ reaction. It shows a broad resonance ($\Gamma \approx 300$ keV) at a proton energy of 650 keV with a scattering cross section of about 60 mb sr^{-1} [10]. The reaction is induced almost uniformly throughout the silicon layer, which represents a proton energy loss of about 40 keV in the 0.55 μm nominal thickness of the silicon layer. To obtain an incident energy of 650 keV, the 970 keV proton beam passed through a uniform nickel foil 2.5 μm thick placed 13 mm in front of the target. The nickel foil was mounted on a small tube to prevent backscattering toward the detectors.

The 3.7 MeV α particles were detected at 150° with a 25 mm^2 silicon surface barrier detector subtending a solid angle of 16 msr. It was covered with a nickel foil 1.25 μm thick and a Mylar foil 8 μm thick to stop the backscattered protons and the light produced in the sapphire substrate, since this can no longer be neglected because the silicon layer is thinned down. A second detector at 145° with a very small solid angle (0.1 msr) was used to monitor the incident protons. To prevent channelling and blocking effects of protons, the target was tilted with respect to low index directions in order to misalign the incident beam and the normalization detector. A beam 5 mm in diameter and currents of the order of 150 nA were used. A large liquid-nitrogen-cooled trap in the reaction chamber prevented any hydrocarbon build-up.

Reproducibility of the measurements was frequently checked with a boron-implanted SOS test sample. The relative boron amount was found to be reproducible within 5%. The very low background allowed us to measure boron surface densities as low as 8×10^{12} cm^{-2}. The absolute boron concentration scale was obtained by implanting a well-known dose in a SOS sample without the SiO_2 layer.

Figure 1 shows a typical energy spectrum of a boron-implanted SOS sample. The 0.7 MeV shoulder is due to 3.3 MeV α particles from the $^{18}O(p,\alpha_0)^{15}N$ reaction in sapphire. Because of the stopping power energy dependence, the energy loss in the

Thin Solid Films, 59 (1979) 385–391
© Elsevier Sequoia S.A., Lausanne—Printed in the Netherlands

THE DIFFUSION COEFFICIENT OF BORON IN EPITAXIAL SILICON LAYERS

F. RUDOLF AND C. JACCARD
Institut de Physique, Rue A.-L. Breguet 1, Université de Neuchâtel, CH-2000 Neuchâtel (Switzerland)
M. E. ROULET
Centre Electronique Horloger S.A., CH-2000 Neuchâtel (Switzerland)
(Received September 20, 1978; accepted October 10, 1978)

The boron diffusion coefficient was measured in boron-implanted silicon-on-sapphire wafers 0.55 μm thick. Implanted doses were between 2.2×10^{14} and 1.4×10^{15} cm^{-2}. Diffusions were conducted in the temperature range 900–1050 °C for times of the order of 0.5–13 h. The boron profiles were measured by the nuclear reaction $^{11}B(p, \alpha_1)^8Be$ in conjunction with ion-milling layer removal. Comparison with profile calculations taking into account the boron concentration dependence shows an enhancement factor of 1.1–2.4 with respect to bulk silicon. An Arrhenius law is found for the diffusion coefficient at low concentration, with an activation energy about 20% less than the 3.6 eV value valid for bulk silicon. The diffusion coefficient is found to be depth dependent. The enhancement is related to crystallographic defects.

1. INTRODUCTION

The process of diffusion migration of atoms in epitaxial structures is expected to differ from that in bulk single crystals.

In some epitaxial silicon layers diffusion enhancements of one order of magnitude have been observed[1]. The determination of the boron diffusion coefficient is of fundamental interest in SOS device technology and particularly in process modelling and simulation[2].

The purpose of this study was to investigate boron diffusion in SOS layers and to compare it with the results known for bulk silicon single crystals. Boron diffusion profiles were measured by a proton-beam-induced nuclear reaction analysis and successive layer removal technique. A similar method has been used recently by Akasaka *et al.*[3] A computer simulation of boron profiles in bulk silicon which accounts for the well-known concentration dependence was used[4] in order to determine the enhancement due to crystalline defects in SOS layers.

2. EXPERIMENTAL

Intrinsic ⟨100⟩ SOS samples 0.55 μm thick from Union Carbide were randomly implanted at room temperature with 40 keV boron ions through SiO_2. The oxide thickness of 0.135 μm is equal to the calculated projected range of 40 keV boron ions in this material[5] and is in close agreement with experimental data[6]. This